Intercomparison and Potential Synergies of Three Methods for Weather Radar Antenna Pointing Assessment

PATRICIA ALTUBE

Meteorological Service of Catalonia, and Department of Astronomy and Meteorology, University of Barcelona, Barcelona, Spain

JOAN BECH

Department of Astronomy and Meteorology, University of Barcelona, Barcelona, Spain

ORIOL ARGEMÍ, TOMEU RIGO, AND NICOLAU PINEDA

Meteorological Service of Catalonia, Barcelona, Spain

(Manuscript received 31 March 2015, in final form 26 November 2015)

ABSTRACT

Three methods for estimation of the weather radar antenna azimuth and elevation pointing offsets are compared. Two of the methods reviewed use the known location of the sun as a reference. The first of these methods is based on an offline scan of the sun disk. The second method detects and characterizes solar interferences in operative scans. The third method consists of correlating measured ground clutter echoes with echoes simulated using a high-resolution digital elevation model. The main objectives are to review the characteristics in each case, studying their performance in actual operative conditions, and to examine the reasons for the discrepancies between the reported pointing bias estimates, with the aim of laying the groundwork for an optimized individual or combined application and interpretation of the methods. Daily pointing biases estimated through the sun-scanning procedure in a dedicated one-month, short-term campaign are the base for the intercomparison. When applied to the three weather radars operated by the Meteorological Service of Catalonia, the short-term study reveals the advantages and limitations of the methods. A one-year, long-term analysis serves to confirm and clarify the discrepancies inferred from the short-term study and highlights how the antenna position at the time of the measurement may influence the pointing bias estimates. Based on the long-term results, a combination of the two sun-based methods for detection and simultaneous quantification of the pointing bias and the system leveling error is discussed.

1. Introduction

Weather radar calibration comprises characterization of the transmit–receive chains (system losses, transmit pulse shape and duration, peak power, receiver curve) and antenna-related features (gain, beam shape, radome losses). Nevertheless, antenna boresight alignment and pedestal leveling status assessment have also been traditionally included in the radar calibration procedures as they are critical for georeferencing radar-measured variables (Vega et al. 2012; Gekat et al. 2004); the accuracy of the antenna alignment constitutes a basic quality factor for primary data and downstream products. For instance, an antenna pointing error of 0.2° at 200 km produces an approximately linear displacement of 700 m, which for many applications may be relevant either in the horizontal or vertical plane. Examples of the above-mentioned error include echo height computing for hail probability assessment (Delobbe and Holleman 2006), topographical beam blockage correction (Bech et al. 2003), and precipitation estimates in small mountain basins for landslide or debris-flow forecasting (Berenguer et al. 2015).

These examples point out the importance of routine checks of the weather radar antenna pointing accuracy. Calibration of the absolute (mechanical and boresight) bearing requires an external target of precisely known location. Common practice calibration methods (see, for

Corresponding author address: Patricia Altube, Meteorological Service of Catalonia, Berlin 38-48, 08029 Barcelona, Spain.
E-mail: paltube@meteo.cat

DOI: 10.1175/JTECH-D-15-0075.1

instance, Manz et al. 2000) rely on either active targets (e.g., directive antennas, transponders, exoatmospheric sources) or fixed-ground and elevated passive targets (e.g., radio tower, reflector mast, orographic perturbations, balloon-/aircraftborne reflectors). Calibration using balloon- or aircraft-mounted targets as reference requires interruption of the radar operation. In addition, if frequent checks are required, then these methods may be logistically and economically costly. On the other hand, ground targets are usually not suitable for elevation calibrations (Divjak et al. 2009). However, Delrieu et al. (1995) developed an algorithm for characterization of the mountain echoes detected by a ground-based weather radar and successfully used the clutter field as reference for estimation of the azimuthal antenna pointing accuracy. A fully automatic extension of the procedure is described in Rico-Ramírez et al. (2009).

The use of weather radars in national and more recently in regional networks has increased awareness and efforts toward the establishment of common procedures and standards in data quality and calibration (Saltikoff et al. 2010; Huuskonen 2001; Huuskonen et al. 2009; Chandrasekar et al. 2014). In this regard, the sun constitutes a well-known, reliable, and worldwide-available exoatmospheric target that can be used as reference for a number of calibration purposes. The use of the sun for offline inspection of weather radar system gain and antenna pointing accuracy has been thoroughly discussed and is currently of widespread employment; see, for instance, Whiton et al. (1976), Frush (1984), Pratt and Ferraro (1989), Eastment et al. (2001), Tapping (2001), Leskinen et al. (2002), and Puhakka et al. (2004). Furthermore, Darlington et al. (2003) showed that the antenna pointing accuracy in azimuth could be monitored on a regular basis from solar signatures detected in radar operational scans. Along these lines, Holleman and Beekhuis (2004) presented a fully automatic procedure for online and simultaneous sun-based monitoring of weather radar antenna alignment and receiver chain calibration. Subsequently, various developments and applications of the technique have been addressed by Huuskonen and Holleman (2007), Frech (2009), Holleman et al. (2010b,a), Muth et al. (2012), and Huuskonen et al. (2014).

Within this framework, testing available antenna alignment monitoring procedures has revealed to be potentially useful for weather radar communities requiring high-quality data observations. In the present work, both the offline and the automatic sun-based methods and the online mountain clutter method are examined and intercompared. All three methods have been implemented and are operative for the weather radar network of the Meteorological Service of Catalonia (SMC). In the upcoming sections, the weather radar network and data are introduced, followed by a detailed description of the operation and characteristics of each of the three antenna pointing methods. The intercomparison is tackled by first analyzing the performance of the methods and identifying the discrepancies in the pointing biases reported in a one-month short-term campaign during which the offline sun-scan method was run on a daily basis. The results collected in a one-year-long period are then studied, based on the measurement conditions and on the procedure followed by each of the methods, to understand and discuss the reasons for the discrepancies found in the short-term analysis.

TABLE 1. Coordinates of the XRAD radar systems and scanning elevations for the short-range volumetric PPI task in each case.

Radar	Location	Height (m MSL)	Elevations (°)
CDV	41.6°N, 1.4°E	825	(0.6, 0.8, 1, 1.3, 1.7
LMI	41.1°N, 0.9°E	910	2, 3, 4, 5, 6, 8, 10
PDA	41.9°N, 3.0°E	542	13, 16, 21, and 27)

2. Data

The results analyzed in this study are derived from the data collected by three C-band (5.3-cm wavelength) single-polarization Doppler weather radars of the SMC network (XRAD) covering the northeastern area of the Iberian Peninsula: Creu del Vent (CDV), La Miranda (LMI), and Puig d'Arques (PDA). The three radars display similar technical and scanning characteristics. Their nominal antenna beamwidths are 1.10° and 1.20° in the horizontal and vertical planes, respectively, with a precision of ±0.05°. These radar systems perform, on a 6-min basis, a long-range single-PPI scanning task at 0.6° elevation and a short-range, dual PRF, multiple-PPI volumetric scan. Short-range PPI scans are preset at fixed elevations ranging from 0.6° to 27° (see Table 1). The sampling settings result in an azimuthal resolution of 1°. The typical XRAD antenna system is based on a C-band linear polarization feed design (manufactured by ORBIT Co.). It comprises an antenna/feed unit and an azimuth/elevation tracking pedestal with an outdoor controller hosted in the radar rack. The antenna/feed unit consists of a 3.8-m parabolic main reflector with a pyramidal horn antenna. The feed horn is attached with an offset from the center of the disk. This configuration, in comparison to a Cassegrain configuration, reduces the sidelobes in the radiation pattern. The antenna disk is mounted on an elevation-over-azimuth positioner, assembled on a base raiser, that allows for independent movements in azimuth and elevation with an orthogonality error

TABLE 2. Intercomparison of relevant characteristics of GC, SI, and SC methods as implemented for the XRAD radar network.

Method	Online	Precipitation immune	AP immune	Elevation(s) (°)	Accuracy (azimuth/elevation) (°)	Quality indicator
GC	Yes	No	No	0.6	0.50/0.10	Max correlation coefficient
SI	Yes	≈Yes	≈Yes	0.6–8	0.05/0.05	RMSE of fit/error of estimates
SC	no	yes	yes	20–60	0.10/0.10	Peak power SNR/fit error

of 0.04°. Manufacturer specifications assign the pointing system an accuracy of 0.03°.

Atmospheric radio propagation conditions during the period studied have been determined based on radiosonde measurements. Soundings are carried out daily at the Barcelona, Spain, rawinsonde station (WMO code: 08190) (41.38°N, 2.12°E; 98 m MSL) using Meteomodem M10 sondes. Launches are programmed twice a day, at 1200 and 2400 UTC. The soundings include surface data at the station location and temperature and humidity measurements at significant and mandatory levels. Radiosonde daily data are used to operationally monitor atmospheric radio propagation conditions by calculating the vertical refractivity gradient of the first kilometer of air (VRG_{1000}) and a ducting index (I_D) in order to detect the occurrence of anomalous propagation events (see Bech et al. 2007 for details).

3. Overview and implementation of the methods

In this section, the three methods for monitoring weather radar antenna pointing accuracy are described in detail. Table 2 compiles the main characteristics of the methods as implemented for the XRAD radar network.

a. Ground clutter returns (GC method)

In the first method (GC), the fixed structures of ground clutter echoes observed in radar image scans at low elevations are compared to ground clutter returns modeled using a high-resolution digital terrain elevation model (DTEM). The module running the GC method at the SMC is part of a set of radar monitoring tools implemented by the Centre of Applied Research in Hydrometeorology [Centre de Recerca Aplicada en Hidrometeorologia (CRAHI)] in Barcelona (Sánchez-Diezma Guijarro 2001; Sánchez-Diezma Guijarro et al. 2002).

The DTEM used for the ground clutter field simulations has a grid resolution of 30 m and a resolution of 1 m in elevation. Considering clear-air and standard atmospheric propagation conditions, ground clutter reflectivity fields are simulated for a collection of antenna elevations using the algorithm by Delrieu et al. (1995). The algorithm models the interaction with topography of three-dimensional electromagnetic pulses. The resolution volume of the radar beam is modeled by a Gaussian angular power pattern and a range weighting function as proposed in Doviak and Zrnić (2006).

Simulated fields are available for an elevation range of ±3° at 0.02° steps. These simulations are correlated with the observed field, built as the average of the daily set of clutter reflectivities collected at 0.6° scans. In addition, predicted fields are azimuthally rotated at 0.1° steps to compute correlations for azimuth lags in a ±3° range. The combination of elevation and azimuth lags yielding the maximum correlation coefficient represents an estimate of the antenna pointing biases in both directions. To achieve collocation of the simulated and observed clutter bins for computation of the correlation coefficient, the simulated field is averaged to the nominal resolution of the PPI field (1.0° in azimuth and 1 km in range) and the observed field is spline interpolated to the locations of the simulation.

The antenna pointing offset estimates for XRAD radars are available online on a daily basis. Approximate accuracy limits of the method reported by the GC module developers are 0.5° in azimuth and 0.1° in elevation. Hence, the GC method as implemented at the SMC is aimed at quantifying elevation antenna pointing errors while only suitable for the detection of large pointing errors in azimuth. Because of the 1.0° nominal azimuthal resolution of the fields, small inaccuracies in the simulation parameters may result in inaccuracies of up to 0.5° in the estimated azimuth pointing biases. As an example, Fig. 1 shows a simultaneous change in the GC reported biases for all XRAD radars when, in December 2014, the parameters of the long-range scanning

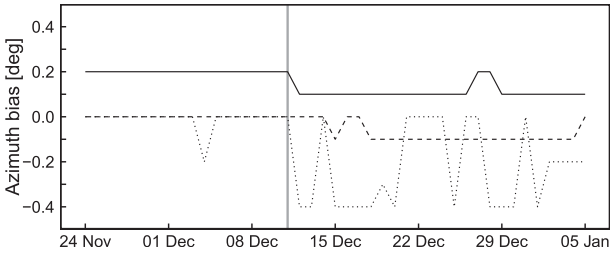

FIG. 1. Azimuthal pointing biases reported by the GC method before and after a change in the nominal resolution of the scanned radial on 11 Dec 2014: CDV radar (solid line), LMI radar (dotted line), and PDA radar (dashed line).

task were modified to change the actual radial resolution of 0.8° to the desired nominal value of 1.0°.

In accordance with the accuracy limits, the operative module provides the values of the estimates rounded to 0.1° precision both in azimuth and elevation. Since no classification of the observed ground clutter echoes is applied, the accuracy of the pointing bias estimates is conditioned by precipitation or anomalous propagation conditions so these factors must be monitored to warrant valid results.

b. Solar interferences (SI method)

The second procedure for online monitoring of antenna alignment (SI) uses solar interferences detected in operational scans (Holleman and Beekhuis 2004). Online application of the SI method requires automatic detection of solar artifacts in polar reflectivity data. A theoretical model for the power of the solar signal is fitted to the collection of solar observations. The model describes the detected power dependent on the relative displacement between the antenna position reading and the sun-disk center. Inversion of the model yields an estimation of the antenna pointing biases in azimuth and elevation (Huuskonen and Holleman 2007). The model inversion also provides estimates of the peak solar power and the sun image scanning widths in azimuth and elevation (Holleman et al. 2010b; Huuskonen et al. 2014).

The SI method implemented at the SMC is adapted to the midrange data (50–130 km) available from the XRAD weather radar network (Altube et al. 2015). Solar interferences are detected daily during sunrise and sunset, both in long- and short-range scans, at antenna elevations ranging from 0.6° to 8°. The original algorithm was modified to minimize the effect of precipitation in the characterization of the detected solar signal, and a methodology for removal of strong outlying observations is applied. Atmospheric anomalous propagation conditions may lead to an inaccurate positioning of the sun with respect to the antenna, mainly for observations collected at low elevations. However, in most cases, its effect upon the retrieved pointing biases lies within the accuracy limits of the method (see section 4), likely because the majority of the observations considered for the model fit remain unaffected. The accuracy of the method is better than 0.05° if the number of observations to be fitted is above approximately 20 (Altube et al. 2014). The uncertainties of the estimated pointing biases, obtained from the covariance matrix of the linear least squares fit, may be considered indicative of the quality of the dataset since they take into account the spread and distribution of the observations (Bevington and Robinson 1969, section 6.4).

c. Sun scan (SC method)

The last of the methods considered (SC) is based on an offline scan of the sun disk and is implemented commercially by several weather radar manufacturers and is a common application in routine technical maintenance tasks. A sun calibration utility, supplied within the radar software package, outputs the signal-to-noise ratio (SNR) data resulting from a sector scan around the expected position of the sun. The utility itself uses the local computer time to calculate the current solar position and controls the antenna scan attending to the user specifications. In the data processing stage, SNR data are thresholded above a user-specified level and a 2D second-order polynomial fit is applied to obtain estimates of the peak solar SNR as well as the sun image width. Data with an SNR value of 3 dB or more under this estimated peak power are then discarded, and a second 2D polynomial fit gives the solar position estimates in azimuth and elevation. Comparison of these position estimates with the solar position as derived from local time identifies antenna pointing offsets (Vaisala 2014, chapter 11).

In the case of the XRAD, the SC routine is configured to perform the sun scan in a sector spanning 4° by 4° in azimuth and elevation with a resolution of 0.2°. The sector is scanned azimuthally, starting below the expected solar elevation and stepwise moving upward. The SC utility corrects for the apparent continuous motion of the sun during the sector scan, recalculating the solar position at the beginning of each sweep and subtracting the difference from all angles in that sweep. Within the specified angular resolution bins, 64 samples are taken at a PRF of 1000 Hz and all range bins farther than 20 km away from the radar are averaged to compute the corresponding SNR value.

The accuracy of the SC-estimated biases depends on the accuracy of the sun-disk center position estimate and on the accuracy of the solar position estimated from the sector scan data processing. The accuracy error of the sun center position is below 0.01° for an error of the order of few seconds in the local time reading (Vaisala 2014, section 3.5). The accuracy of the peak solar power position depends on a number of factors, such as measuring elevation, quality, and number of valid data or solar emission pattern. Most of these factors are quality controlled by the utility itself while running, through the evaluation of indicators such as the image area covered by valid data, the SNR of the peak power, and the root-mean-square error (RMSE) of the fit. Given the similarities in the data collection and fitting process, it is estimated that the peak position accuracy will be around 0.05° as in the case of the SI method. Under these

considerations, the accuracy of the SC method is assumed to be better than the 0.1° value given by the resolution of the sun scan dataset.

Routine checks of the XRAD radars' antenna alignment by means of the SC method are carried out bimonthly by technicians. Following the recommended procedures established for the XRAD, SC measurements are taken only on clear-air days and the utility is run twice, in the morning and in the afternoon, always when the sun is at an elevation between 20° and 60°. These procedures are set to ensure the pointing bias estimates are not affected by precipitation or anomalous refraction conditions. During February–March 2014, a dedicated SC campaign was carried out to assess the stability of the method and the resulting antenna positioning errors. The SC utility was run in the morning and in the afternoon on a daily basis (excluding weekend and rainy days), summing up a total of 22 days. Measurement times were fixed, generally around 1000 and 1400 UTC, to ensure that morning/afternoon solar zenithal positions were similar and above 20° and that the solar azimuthal positions would not vary strongly throughout the campaign.

4. Results

In the following, the analysis and comparison of the antenna pointing monitoring methods is presented, based on the results of their application to the XRAD radars for the period from April 2013 to March 2014, with particular insight into the dedicated short-term campaign during February–March 2014.

Pointing bias estimates by the GC method were selected, keeping the results corresponding only to days with clear skies and standard conditions. Days with standard atmospheric propagation conditions were identified using VRG_{1000} and I_D data from radiosonde observations, by application of the thresholds tabulated in Bech et al. (2007). Precipitation accumulation maps (Trapero et al. 2009) for the selected days were further inspected to discard those for which any precipitation was present. Figure 2 shows the results of the classification: 13.5% of the total number of days of the long-term period was identified as clear-air days with standard propagation conditions.

Based on this classification, the influence of precipitation and anomalous propagation on the pointing biases estimated by the SI method was investigated. SI results were split into four groups, corresponding to different atmospheric conditions: clear air and standard propagation, precipitation only, anomalous propagation only, and both precipitation and anomalous propagation. Resulting statistics of the classification are shown in

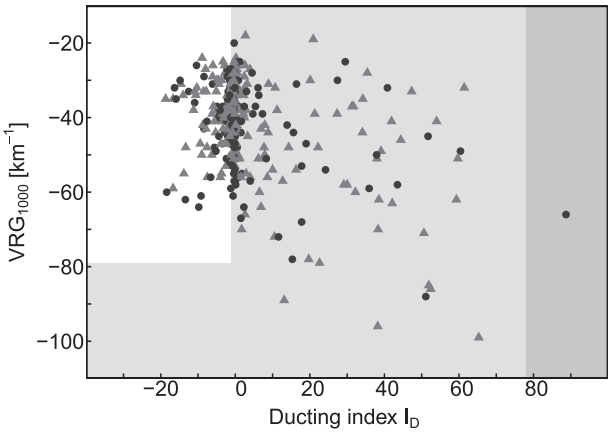

FIG. 2. Atmospheric propagation conditions at 1200 UTC from April 2013 to March 2014. Values of I_D and VRG_{1000} derived from radiosonde measurements are used to classify the daily propagation conditions: standard (white), superrefraction (light gray), and ducting (dark gray). Triangles represent clear-air days, while black dots represent days for which any precipitation was present.

Fig. 3 for the PDA radar. A statistical test comparing the mean pointing biases reported under clear-air and standard propagation conditions with the mean reported under the other conditions showed that the differences are not significant. Only the combination of precipitation and anomalous propagation seemed to have a slight effect on the elevation pointing offsets, but the bias was minimal, around 0.01°, below the accuracy limits of the SI method.

Therefore, the quality selection of SI results was based on the number of solar observations available for the fit and on the uncertainty of the parameters derived from the fit. The maximum errors allowed for an accepted result were 0.05° in the pointing offsets and 0.1° in the width estimates, and a minimum number of 20 solar observations was required.

a. Short-term campaign

An example of the comparison of the antenna pointing biases obtained from the three methods for the short campaign period from 10 February to 14 March 2014 is shown in Fig. 4 for the CDV radar. Results from morning and afternoon measurements using the SC utility were averaged into a single daily estimate by application of a mean weighted by the fit error. First inspection of the figure indicates that the precision of the estimates by the sun-based methods, SI and SC, was below 0.05°. However, a systematic difference of about −0.1° between the biases from the SI and SC methods was perceivable, both in azimuth and elevation.

As reasoned in an upcoming section, section 4c, the precision of the biases estimated through the GC method is below the 0.1° output precision given by the

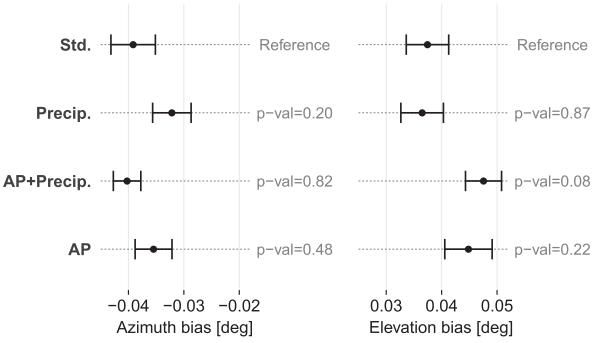

FIG. 3. Mean antenna pointing biases estimated by the SI method for the PDA radar, classified according to the atmospheric conditions: clear air and standard propagation (Std), precipitation only (Precip), anomalous propagation only (AP), and both precipitation and anomalous propagation (AP+Precip). Error bars illustrate the standard error of the mean. Only SI estimates derived from fits to solar observation datasets larger than 20 are considered. Given are the p values corresponding to t-value tests of the difference between the mean under standard conditions and the means under nonstandard conditions. Values of p larger than 0.05 (95% level) indicate a nonsignificant difference with respect to the standard conditions.

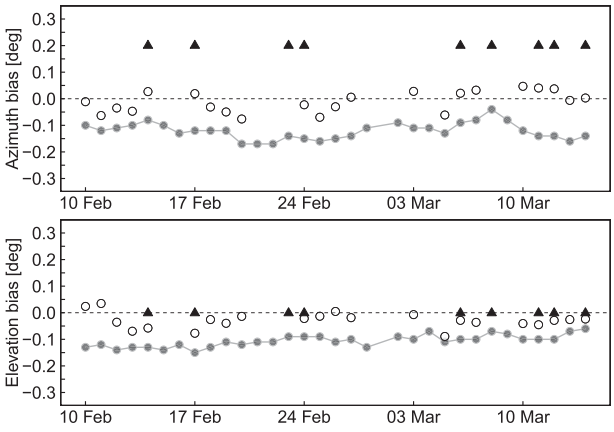

FIG. 4. Antenna pointing bias estimates in (top) azimuth and (bottom) elevation for the CDV radar in the period from 10 Feb 2014 to 14 Mar 2014. Results for the three different antenna alignment methods are displayed: GC method (black triangles), SI method (gray circles), and SC method (white circles). For the sake of clarity, the SI method results are shown connected by a line.

operative module and therefore the day-to-day variability of the estimates is not perceivable in the presented results. This is not critical in the case of the azimuth biases because the correlation coefficients between the observed and simulated clutter fields are calculated in 0.1° steps. However, for the elevation biases, an output precision of 0.01°, finer than the one currently provided by the operative module, would be desirable for adequate quality control.

EAST/WEST SPLITTING

For a more detailed insight, the SC estimates obtained in the morning and in the afternoon were separately analyzed. SC results were classified into east (SC-E) and west (SC-W) according to the azimuthal position of the antenna with respect to north (0°) at the time of the measurement. SC-E measurements were taken at azimuthal positions between 140° and 160°, while SC-W measurements were taken between 210° and 240°.

In the case of the SI method, computation of separated bias estimates for the east and west positions was also possible. SI estimates were computed again, differentiating between east (SI-E) and west (SI-W) by application of the method to sun interferences detected at either sunrise or sunset, respectively, during three consecutive days. Conditioned by the local solar sunrise and sunset positions for the considered dates, SI-E solar observations were collected at azimuthal positions between 95° and 115° and SI-W observations at positions between 225° and 265°.

As seen in Fig. 5, this classification revealed a systematic difference between the elevation biases measured at the east and west positions of the CDV radar antenna. The east–west offset was approximately +0.09° for the SC method and reached +0.16° for the SI method. In turn, no significant difference in the azimuth bias estimates was noticeable. These results altogether indicated a possible inclination of the antenna rotation plane with respect to the horizontal plane, often associated with pedestal leveling errors (Frech 2009). The possibility of the east–west differences being related to a misalignment between the sun-disk center and the ''microwave center'' (Chandrasekar et al. 2014) was discarded given the length of the time period studied (of the order of the solar rotation period) and the stability of the differences found.

Table 3 presents the statistics of the biases estimated during the short-term campaign period and for all three XRAD radars. Examination of the results showed that application of the SI method to all sun interferences, collected at both sunrise and sunset, yields bias estimates that are approximately the average of those biases computed separately from the east and west interferences. In addition, a significant east–west offset in the elevation biases from the SI and SC methods was detected also for the PDA radar.

The average SNR values of the peak solar signal derived from the SC method were, in linear units, three for LMI, four for CDV, and six for PDA. In the cases of LMI and CDV, a slightly larger day-to-day variability of azimuth bias estimates is expected; in azimuthal direction solar features are smoothed and attenuated due to the scanning motion and the precision of the estimates may be affected by the low sensitivity. Note, however, the remarkably larger variability in the SC

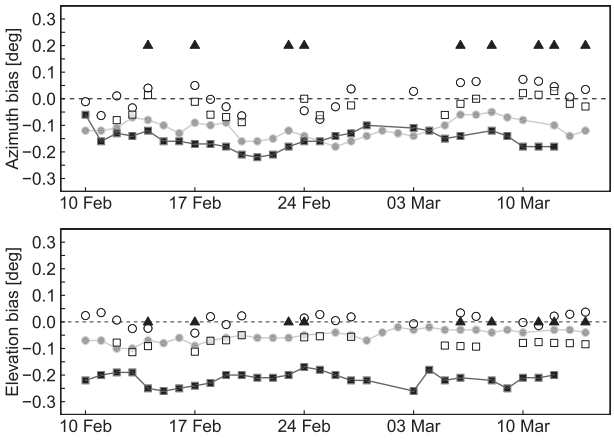

FIG. 5. As in Fig. 4, but with the estimates from sun-referenced methods separated according to the east–west azimuthal position of the antenna at the time of the measurement: GC (black triangles), SI-E (light gray circles), SI-W (dark gray squares), SC-E (white circles), and SC-W (white squares).

azimuth biases for the LMI radar. This was attributed to the presence of a significant backlash in azimuth, associated with a severe wearing of the azimuth resolver gear cogs. This problem was detected in due course and solved by replacement of the resolver on the 14 April 2014.

The radar sensitivity may also affect the precision of the SI method estimates (Altube et al. 2015) but is not as clearly reflected in the short-term statistics of the estimates (Table 3) due to the aforementioned quality selection of the results. Indeed, accounting for all results collected in the one-year-long time period, the valid daily SI results remaining for the LMI radar after thresholding was reduced to a 55% of the total, while remaining valid results for CDV and PDA radars were of 75% and 84%, respectively.

Finally, the clear discrepancies of the GC azimuth biases with respect to the sun-based methods are within the accuracy limit of 0.5° established for the GC method.

b. *SI and SC methods: Antenna system leveling*

The east/west splitting for both the SI and SC methods as described in the previous section allowed, on a long-term analysis, to examine the dependence of the elevation pointing biases (δ_θ) upon the azimuthal position of the antenna (ϕ). In the presence of a leveling error, this dependence is expected to be of the type

$$\delta_\theta = \delta_{\theta,0} + \beta_0 \cos(\phi - \phi_0), \quad (1)$$

where β_0 is the angle of inclination between the rotation axis and the vertical; ϕ_0 is the azimuthal direction of the inclination with respect to north; and $\delta_{\theta,0}$ is a systematic elevation error, which includes the antenna axis elevation offset and any (boresight) misalignment between this axis and the electrical axis. Equation (1) is an adaptation of the model presented in the exhaustive work by Muth et al. (2012).

The east–west implementation of SI method was applied from 1 April 2013 to 31 March 2014. The collection of 3-day sunrise or sunset sun interferences was positioned within azimuth stripes of 5°–10° width and the median position was used as reference for the retrieved bias estimates. The time period considered covered the whole solar cycle of local sunrise and sunset azimuthal positions, which spanned the ranges from approximately 55° to 125° and from 230° to 300°, respectively. Also included in the analysis were the SC method results, encompassing both the bimonthly technical tests throughout this period and the short-term campaign results presented in the previous section.

Figure 6 shows the azimuthal dependence of the elevation biases retrieved through the SI and SC methods for the CDV and PDA radars. The LMI case is not presented because no consistent difference between the east and west pointing biases was found, not in the short-term campaign nor in the long-term period. For the CDV and PDA radars, a difference between east and west results was appreciable in both cases and a sinusoidal dependence was perceived when all results were considered together. Nonlinear least squares fits of the leveling error model in Eq. (1) were applied independently to SI and SC estimates (Fig. 6). The model parameters retrieved in each case are detailed in Table 4.

TABLE 3. Mean and standard deviation of antenna pointing bias estimates for the XRAD radars from 10 Feb to 14 Mar 2014. Results from sun-referenced methods are separated according to the east–west azimuthal position of the antenna at the time of the measurement. In the case of the SI method, the results of the application of the method to the east and west interferences together are also shown for comparison.

Radar		GC	SI	SI-E	SI-W	SC-E	SC-W
CDV	Azimuth (°)	0.2 ± 0.0	−0.12 ± 0.03	−0.11 ± 0.03	−0.15 ± 0.04	0.01 ± 0.05	−0.03 ± 0.04
	Elevation (°)	0.0 ± 0.0	−0.11 ± 0.02	−0.05 ± 0.02	−0.21 ± 0.02	0.01 ± 0.02	−0.08 ± 0.02
LMI	Azimuth (°)	0.2 ± 0.1	−0.27 ± 0.02	−0.25 ± 0.03	−0.31 ± 0.02	0.02 ± 0.12	0.05 ± 0.15
	Elevation (°)	−0.4 ± 0.0	−0.14 ± 0.02	−0.16 ± 0.02	−0.12 ± 0.02	−0.04 ± 0.01	−0.01 ± 0.02
PDA	Azimuth (°)	0.0 ± 0.0	−0.01 ± 0.01	0.02 ± 0.01	−0.05 ± 0.02	−0.06 ± 0.02	−0.07 ± 0.02
	Elevation (°)	0.2 ± 0.0	0.02 ± 0.01	−0.01 ± 0.01	0.07 ± 0.02	0.04 ± 0.02	0.12 ± 0.02

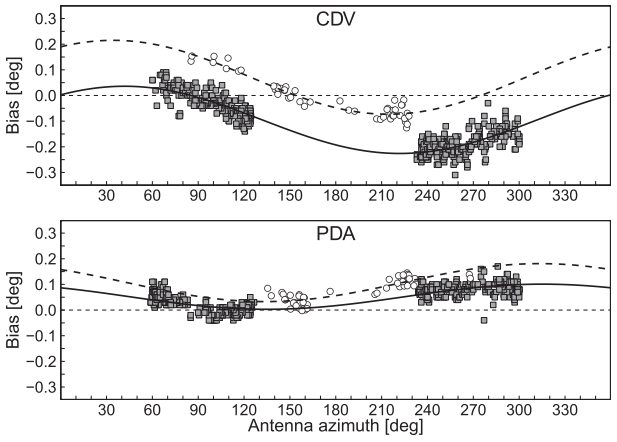

FIG. 6. Elevation pointing biases estimated for the (top) CDV and (bottom) PDA radars from 1 Apr 2013 to 31 Mar 2014 as a function of the azimuthal position of the antenna: SC (white circles) and SI (gray squares) method estimates. Lines represent the resulting leveling error model [Eq. (1)] fits to the SC (dashed line) and SI (solid line) estimates.

Outcomes of the fits indicated that a significant inclination of approximately 0.14° was present at an azimuth within 30°–40° from north for the CDV radar. Although the noteworthy difference between SI and SC systematic offset estimates was quantified around +0.15°, the leveling errors derived from both methods were in accordance. In the case of the PDA radar, the inclination of about 0.05° found at an azimuth around 315° was not significant given the precision of the SI and SC methods and was positioned within the margins accepted for the antenna pointing accuracy. The difference between the SI and SC offset estimates for the PDA radar was minor, around +0.05°. The reason for the differences between the SI and SC offsets is discussed in section 4d.

c. GC method: Precision and influential clutter bins

The GC method calculates the Pearson correlation coefficient (r) between the observed (Z^{o}) and simulated (Z^{s}) reflectivities of ground clutter echoes for different combinations of δ_ϕ and δ_θ azimuth and elevation pointing biases:

$$r(\delta_\phi,\delta_\theta)=\frac{1}{N-1}\sum_{\phi}\sum_{r}\left[\frac{Z^{o}_{r,\phi}-\overline{Z^{o}}}{\sigma^{o}}\right]\left[\frac{Z^{s}_{r,\phi}(\delta_\phi,\delta_\theta)-\overline{Z^{s}}}{\sigma^{s}}\right], \quad (2)$$

where N is the number of clutter bins considered; $\overline{Z^{o}}$, $\overline{Z^{s}}$ are the average reflectivities; and σ^{o}, σ^{s} are the standard deviations of the observed and simulated ground clutter reflectivity fields, respectively. Terms (r, ϕ) are range and azimuth positions indexing each particular clutter bin within the fields, respectively.

TABLE 4. Leveling error model [Eq. (1)] parameters and their errors as retrieved for the CDV and PDA radars in a nonlinear least squares fit of the elevation bias estimates from the SI and SC methods.

	Data	Offset ($\delta_{\theta,0}$) (°)	Inclination (β_0) (°)	Direction (ϕ_0)(°)
CDV	SI	−0.097 ± 0.002	0.132 ± 0.004	42 ± 2
	SC	0.07 ± 0.01	0.15 ± 0.01	32 ± 4
PDA	SI	0.052 ± 0.001	0.049 ± 0.002	315 ± 3
	SC	0.11 ± 0.02	0.07 ± 0.02	313 ± 17

The function $r(\delta_\phi, \delta_\theta)$ has a maximum at $(\delta_{\phi,0}, \delta_{\theta,0})$; the latter constitute the antenna elevation and pointing biases reported by the GC method. Table 5 gives the average and standard deviation of the maximum correlation coefficient for the XRAD radars during the long time period from 1 April 2013 to 31 March 2014.

In the case of the XRAD, it has been estimated that the sensitivity of r in the neighborhood of the maximum is of the order of $dr/d(\delta_\phi) \approx 0.1\ \text{deg}^{-1}$ for azimuth biases and $dr/d(\delta_\theta) \approx 0.3\ \text{deg}^{-1}$ for elevation biases. These sensitivities combined with the standard deviation of the maximum correlation coefficient (see Table 5) indicate that the minimum precision (understood here as the maximum day-to-day variability) of the GC results is around ±0.1° in azimuth and ±0.03° in elevation for the CDV and PDA radars and around ±0.3° in azimuth and ±0.1° for the LMI radar.

Based on Eq. (2), relevant quantities for the calculation of significant correlation coefficients include the number of points/bins considered and the variance of their reflectivities. These quantities, given for the XRAD radars in Table 5, indicate that the minimum r required for a significant correlation is higher for the LMI radar than for the PDA and CDV radars. In addition, the two bracketed factors in Eq. (2) are the standard scores of the observed and simulated clutter bins, indicating that bins with a reflectivity with a large deviation with respect to the mean value constitute influential points and have the potential to resolve the value of r. In Fig. 7 polar maps of the standard score of the observed clutter fields at an elevation of 0.6° are displayed for each of the XRAD radars considered. Among these standard score fields, influential bins have been identified as those with a reflectivity value beyond the $\pm 1.5\sigma$ interval around the expected value.

As shown in Fig. 8, for the LMI radar few influential bins with large standard scores determine the value of the correlation coefficient. Variability in the observed reflectivity of these bins has a large effect upon the precision, and small inaccuracies in their simulation may bias the method results. These considerations may explain the difference of the GC elevation bias estimates compared to the SI and SC method estimates (Table 3).

TABLE 5. Values of variables relevant for the correlation coefficient calculation and for the performance of the GC method when applied to the XRAD radars.

	CDV	LMI	PDA
Max correlation	0.67 ± 0.01	0.66 ± 0.03	0.789 ± 0.008
Std dev of Z (dB)	≈16	≈10	≈15
No. of bins	≈9600	≈7200	≈8300
Influential bins (%)	17.1	14.8	17.5
Influential azimuth (°)	10–40	10–40	250–270
	330–360	220–240	290–340

In the case of the CDV and PDA radars, influential clutter bins are confined to particular azimuth regions. The biases estimated by the GC method are those corresponding to the azimuth regions in which the influential bins are clustered. Therefore, identification of these azimuth regions is relevant for the interpretation of the GC results, in particular if a pedestal leveling error is present. Influential azimuth ranges for the XRAD radars have been recognized as those with the largest number of influential bins and are specified in Table 5. Note that for the CDV radar, the elevation bias of 0° reported by the GC method (Table 3) coincided with the bias expected when measuring, at low antenna elevations, in the azimuth sector from 330° to 40° when the leveling error detected was taken into account (Fig. 6). Similarly, for the PDA radar, the GC method elevation bias of 0.2° was close to the biases predicted by the leveling error models at azimuthal positions between 250° and 340°.

d. Analysis by antenna elevation

The analysis as a function of the antenna azimuthal position presented in section 4b pointed to the existence of a systematic difference between the elevation offsets measured by the SI and SC methods for the CDV radar. As an example, Fig. 9 shows, for all three radars considered, a comparison of the elevation biases measured through the SI method versus those measured through the SC method. The data points correspond to measurements for which the antenna azimuthal position coincided for both methods (within ±5°). This comparison confirmed that a significant difference between the SI and SC elevation biases was present for both the CDV and LMI radars.

Considering that SI and SC measurements were collected at very different antenna elevation positions (Table 2), the dependence of the estimates as a function of antenna elevation (θ) was examined as the possible reason for the observed differences; a variation of the measured elevation pointing bias dependent on the antenna elevation may be indicative of nonlinearities in the angle conversion by the elevation resolver device (Chandrasekar et al. 2014). In the case of SC method biases, each of which correspond to a fixed elevation measurement, derivation of the dependence was straightforward. However, SI biases resulted from the information provided by sun interferences detected at elevations between 0.6° and 8°. Therefore, solar data were reanalyzed, splitting the interferences first into east and west and then into the different antenna elevations programmed in the scanning task (Table 1). To keep the number of interferences above 20 for each of the sets, the SI method was applied to observations collected within 10-day moving windows. Also, to avoid any inaccuracies in the estimates resulting from solar flux variations throughout these 10-day periods, the power of the solar observations was normalized prior to the fit, scaling it by the detected peak solar power derived from the corresponding daily SI fit (without any splitting).

To extract the azimuth dependence of the biases in the cases of the CDV and PDA radars, the sinusoidal term in Eq. (1) was subtracted from the SI and SC estimates

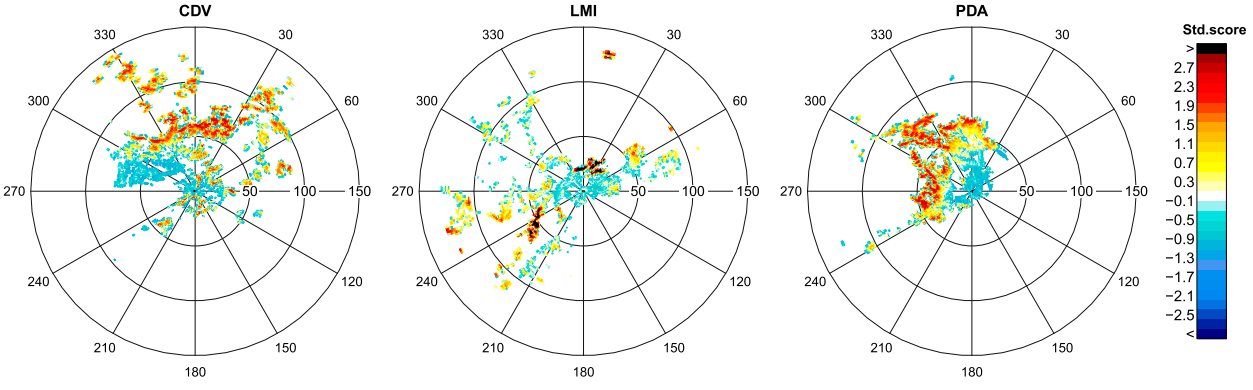

FIG. 7. Polar maps of standard scores computed from the average ground clutter reflectivity field measured during 7 days with clear-air and standard atmospheric propagation conditions in March 2014 at 0.6° elevation for the (left) CDV, (center) LMI, and (right) PDA radars. Radial grid units are degrees from north, and circular grid units are kilometers from the radar site.

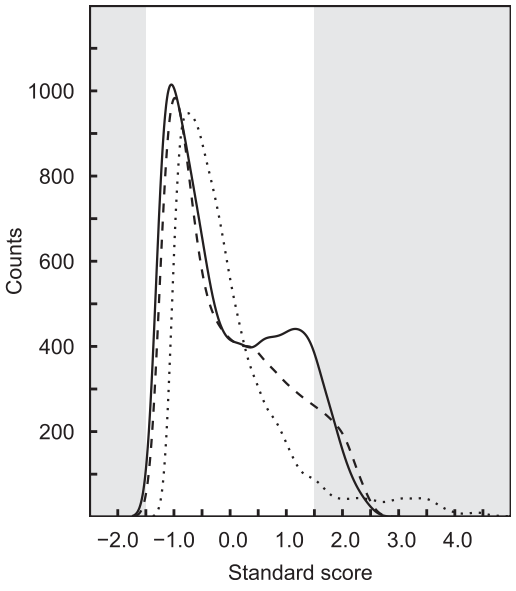

FIG. 8. Histograms of standard scores computed from the bin fields in Fig. 7 for the CDV (solid line), LMI (dotted line), and PDA (dashed line) radars. Gray areas indicate the regions where influential bins are selected.

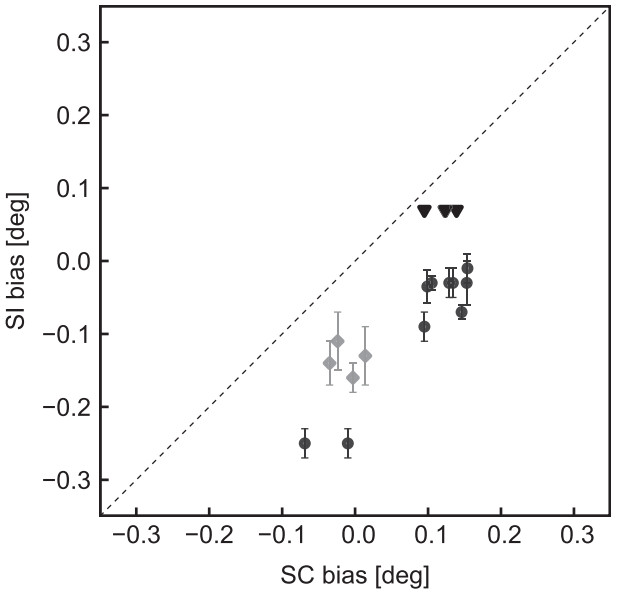

FIG. 9. Comparison of elevation pointing biases estimated for the XRAD radars by the SI and SC methods at coincident azimuthal positions of the antenna: CDV (dots), LMI (diamonds), and PDA (triangles). Bars indicate the uncertainties of the estimates derived from the fit in the SI method.

(δ_θ) using the inclination (β_0) and direction (ϕ_0) angle values derived in the leveling error model fit (Table 4). This assumes that only the constant offset term [$\delta_{\theta,0}(\theta)$] presents a dependence on elevation.

Figure 10 displays the resulting elevation pointing biases as a function of antenna elevation: the SI method estimates at low elevations and the SC method estimates at high elevations. Given the large amount of data available from the SI method, the median value of the estimated biases is displayed at each elevation. Despite the elevation region for which no SC measurements were carried out, in all cases the values of the biases at low elevations showed continuity at high elevations. The biases at low elevations traced an increasing trend with elevation (around 0.01° per degree elevation) for the three radars. In the case of the CDV radar, the increasing trend was also perceptible at a lower rate (around 0.005° per degree elevation) at high elevations. For all cases, the results appeared in agreement with the discrepancy between the offsets found for the SI and SC methods. Even in the case of the PDA, the elevation bias increasing trend at low elevations seemed compensated by a decreasing trend at high elevations, which may explain the absence of a significant difference between the SI and SC estimates.

As observed in Fig. 10 the elevation pointing biases measured for the CDV and LMI radars at high antenna elevations were 0.2°–0.3° different from those measured at low elevations. These results indicate that adjusting the antenna pointing bias based on SC measurements carried out at high elevations may not be appropriate for meteorological applications, in which low elevations are the relevant ones.

5. Summary and conclusions

In the present article, three existing methods for antenna pointing monitoring have been reviewed and comparatively studied. The first method (GC) uses daily observed ground clutter returns as reference. The other methods use the known location of the sun as reference: the first (SC) is based on an offline sun scan, while the second method (SI) uses sun interferences detected in operational radar scans.

GC and SI methods are run online and do not require the interruption of the radar operation. However, the accuracy of the GC method may be compromised by precipitation or anomalous atmospheric propagation conditions, and the precision of the SI estimates depends on the quality and number of the collected solar observations. Both methods estimate the antenna pointing biases at low elevations, which are the most relevant in the georeferenciation and quantification of precipitation. In turn, the SC method is run offline, providing only isolated bias estimates. However, if measurements are taken on clear-air days and at high elevations, as in the presented cases, then the results are assumed unaffected by atmospheric conditions.

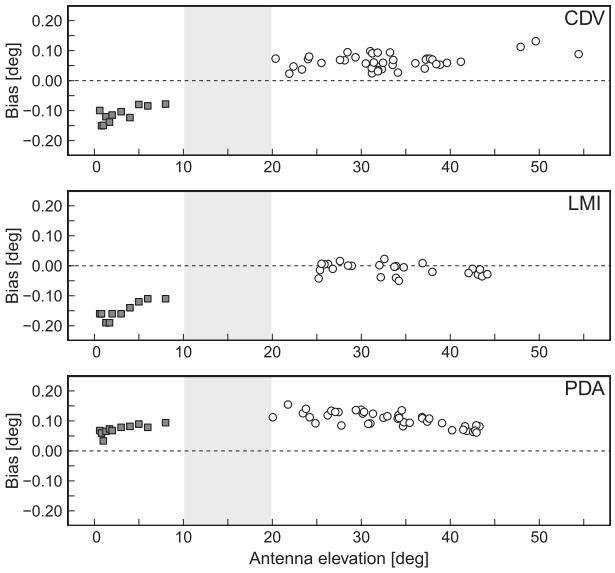

FIG. 10. Elevation pointing biases estimated for the (top) CDV, (middle) LMI, and (bottom) PDA radars as a function of the elevation position of the antenna. Both the SC (white circles) and SI (gray squares) method estimates are shown. Shadowed area indicates the antenna elevation range for which measurements were not available in the case of the SI method nor were routinely carried out in the case of the SC method.

Daily SC measurements carried out during a one-month campaign have made possible a direct comparison of the pointing biases estimated by the methods. The results of this short-term analysis have shown that the day-to-day variability of the bias estimates by the sun-based methods, SI and SC, is below 0.02°. Nonetheless and particularly for the azimuth biases, this precision decreases if the radar sensitivity is close to the peak solar signal level. A remarkably large day-to-day variability in the SC azimuth offset estimates has proven to be indicative of azimuthal backlash, a consequence of the degradation of a mechanical component. In the case of the GC method, the angular resolution of the PPI clutter fields due to sample averaging may compromise the accuracy of the azimuth pointing offsets.

A one-year, long-term analysis of the performance of the methods has pointed out the importance of accounting for the antenna position at the time of the measurement when interpreting the reported pointing biases. For the SI method, east/west splitting of the solar observations and reanalysis of the data has allowed for examination of the elevation biases as a function of the azimuthal position of the antenna and a characteristic dependence has been found, associated with an inclination of the antenna rotation plane with respect to the horizontal plane and attributed to a structural leveling error. Elevation biases reported by the SC method throughout the long-term period have shown an azimuthal dependence in agreement, confirming the leveling error. After subtracting the azimuthal dependence, it has been shown that pointing offset estimates may also present a dependence upon the antenna elevation position. The presence of such a dependence, likely related to a nonlinearity in the resolver angle conversion, even if not very pronounced, may introduce a significant difference between the biases estimated by the SI and SC methods if the measurements of the SC method are performed at high antenna elevations.

For the GC method, the effect of the ground clutter azimuthal distribution has been investigated and for each radar the clutter bins influencing the bias estimates have been defined. For radars with few clutter bins, the correlations computed tend to be less significant, and isolated strong clutter structures may bias the pointing offset estimates and decrease their precision. Two cases of radars for which the influential bins are confined to vast but limited azimuth regions have also been presented. It has been found that at these influential azimuth regions, the GC elevation biases are in accordance with those found for the SC and SI methods when the pedestal leveling error is taken into account.

Overall, the results demonstrate the ability of all three methods to detect severe antenna misalignments in the short term. However, for remote and accurate quantification of both the pointing offsets and monitoring of the system leveling status, a long-term, synergistic application of the sun-based procedures is suggested. Although the proposed methodology requires further validation, the present study has shown that such a combined application may provide pointing bias estimates in an expanded range of azimuth and elevation antenna positions. The range of azimuthal positions of the antenna accessible by SI measurements during a one-year period depends on the latitudinal location of the radar and on the maximum scan elevation (Frech 2009), attending to the local annual solar motion. For most cases, the pointing biases are not measurable through the SI method for both a northerly and a southerly region of azimuthal positions. However, the gap at southerly azimuths can be partially covered by long-term SC measurements programmed in advance. The analysis of SI and SC elevation pointing biases as a function of antenna azimuthal position would serve to separate the leveling error from the systematic alignment offset, if present. In addition, comparison and/or analysis of SI and SC systematic elevation offsets would allow for detecting and estimating differences between the methods related to a dependence upon the antenna elevation position, providing a means for appropriate calibration of the antenna alignment at the chosen elevation.

Acknowledgments. This study was performed under the framework of the Industrial Doctorate Programme partly funded by the autonomous government of Catalonia and the Meteorological Service of Catalonia. Three anonymous reviewers helped to improve the final form of this paper. We are grateful to Prof. Vicente Caselles (University of Valencia) for his valuable comments regarding the terminology of instrumental and methodological errors.

REFERENCES

Altube, P., J. Bech, O. Argemí, T. Rigo, and N. Pineda, 2014: Weather radar online Sun-monitoring in presence of leverage outliers: Five or three parameter model inversion? *Extended Abstracts, Eighth European Conf. on Radar in Meteorology and Hydrology (ERAD)*, Garmisch-Partenkirchen, Germany, DLR, 8.4. [Available online at http://www.pa.op.dlr.de/erad2014/programme/ExtendedAbstracts/015_Altube.pdf.]

——, ——, ——, and ——, 2015: Quality control of antenna alignment and receiver calibration using the sun: Adaptation to midrange weather radar observations at low elevation angles. *J. Atmos. Oceanic Technol.*, **32**, 927–942, doi:10.1175/JTECH-D-14-00116.1.

Bech, J., B. Codina, J. Lorente, and D. Bebbington, 2003: The sensitivity of single polarization weather radar beam blockage correction to variability in the vertical refractivity gradients. *J. Atmos. Oceanic Technol.*, **20**, 845–855, doi:10.1175/1520-0426(2003)020<0845:TSOSPW>2.0.CO;2.

——, ——, and ——, 2007: Forecasting weather radar propagation conditions. *Meteor. Atmos. Phys.*, **96**, 229–243, doi:10.1007/s00703-006-0211-x.

Berenguer, M., D. Sempere-Torres, and M. Hürlimann, 2015: Debris-flow forecasting at regional scale by combining susceptibility mapping and radar rainfall. *Nat. Hazards Earth Syst. Sci.*, **15**, 587–602, doi:10.5194/nhess-15-587-2015.

Bevington, P. R., and D. K. Robinson, 1969: *Data Reduction and Error Analysis for the Physical Sciences*. 3rd ed. McGraw-Hill, 336 pp.

Chandrasekar, V., L. Baldini, N. Bharadwaj, and P. L. Smith, 2014: Recommended calibration procedures for GPM ground validation radars. GPM Tier1 Documentation Draft 9, Global Precipitation Measurement Project, 100 pp.

Darlington, T., M. Kitchen, J. Sugier, and J. de Rohan-Truba, 2003: Automated real-time monitoring of radar sensitivity and antenna pointing accuracy. *31st Conf. on Radar Meteorology*, Seattle, WA, Amer. Meteor. Soc., 7B.6. [Available online at https://ams.confex.com/ams/32BC31R5C/techprogram/paper_63543.htm.]

Delobbe, L., and I. Holleman, 2006: Uncertainties in radar echo top heights used for hail detection. *Meteor. Atmos. Phys.*, **13**, 361–374, doi:10.1017/S1350482706002374.

Delrieu, G., J. D. Creutin, and H. Andrieu, 1995: Simulation of radar mountain returns using a digitized terrain model. *J. Atmos. Oceanic Technol.*, **12**, 1038–1049, doi:10.1175/1520-0426(1995)012<1038:SORMRU>2.0.CO;2.

Divjak, M., and Coauthors, 2009: Radar data quality-ensuring procedures at European weather radar stations. Subproject 1c/1 OPERA/WD/9/1999, OPERA-EUMETNET, 12 pp.

Doviak, R. J., and D. S. Zrnić, 2006: *Doppler Radar and Weather Observations*. 2nd ed. Dover Publications, 592 pp.

Eastment, J. D., J. W. F. Goddard, G. J. Davies, D. N. Ladd, and K. J. Twort, 2001: Boresight pointing calibration for the Chilbolton radar using galactic radio sources and satellite targets. Preprints, *30th Int. Conf. on Radar Meteorology*, Munich, Germany, Amer. Meteor. Soc., P1.2. [Available online at https://ams.confex.com/ams/30radar/techprogram/paper_19854.htm.]

Frech, M., 2009: Towards monitoring and assessing DualPol data quality: Contribution to OPERA WP1.4a; Evaluation of new technologies. OPERA-EUMETNET, 54 pp.

Frush, C. L., 1984: Using the sun as calibration aid in multiple parameter meteorological radar. Preprints, *22nd Conf. on Radar Meteorology*, Zurich, Switzerland, Amer. Meteor. Soc., 306–311.

Gekat, F., P. Meischner, K. Friedrich, M. Hagen, J. Koistinen, D. B. Michelson, and A. Huuskonen, 2004: The state of weather radar operations, networks and products. *Weather Radar: Principles and Advanced Applications*, P. Meischner, Ed., Physics of Earth and Space Environments, Springer, 1–51, doi:10.1007/978-3-662-05202-0.

Holleman, I., and H. Beekhuis, 2004: Weather radar monitoring using the sun. KNMI Tech. Rep. TR-272, 40 pp.

——, A. Huuskonen, R. Gill, and P. Tabary, 2010a: Operational monitoring of radar differential reflectivity using the sun. *J. Atmos. Oceanic Technol.*, **27**, 881–887, doi:10.1175/2010JTECHA1381.1.

——, ——, M. Kurri, and H. Beekhuis, 2010b: Operational monitoring of weather radar receiving chain using the sun. *J. Atmos. Oceanic Technol.*, **27**, 159–166, doi:10.1175/2009JTECHA1213.1.

Huuskonen, A. J., 2001: A method for monitoring the calibration and pointing accuracy of a radar network. Preprints, *30th Conf. on Radar Meteorology*, Munich, Germany, Amer. Meteor. Soc., P1.4. [Available online at https://ams.confex.com/ams/30radar/techprogram/paper_21379.htm.]

——, and I. Holleman, 2007: Determining weather radar antenna pointing using signals detected from the sun at low antenna elevations. *J. Atmos. Oceanic Technol.*, **24**, 476–483, doi:10.1175/JTECH1978.1.

——, M. Kurri, and J. Koistinen, 2009: Harmonized production practices for volume data, low level reflectivity and weather radar wind profile. OPERA-3 Deliverable OPERA_2008_06, OPERA-EUMETNET, 54 pp.

——, ——, H. Hohti, H. Beekhuis, H. Leijnse, and I. Holleman, 2014: Radar performance monitoring using the angular width of the solar image. *J. Atmos. Oceanic Technol.*, **31**, 1704–1712, doi:10.1175/JTECH-D-13-00246.1.

Leskinen, M., P. Puhakka, and T. Puhakka, 2002: A method for estimating antenna beam parameters using the Sun. *Proceedings of the Second European Conference on Radar Meteorology and Hydrology (ERAD): In Conjunction with COST 717 Mid-Term Seminar*, Copernicus, 318–323.

Manz, A., A. H. Smith, and P. J. Hardaker, 2000: Comparison of different methods of end-to-end calibration of the U.K. weather radar network. *Phys. Chem. Earth*, **25B**, 1157–1162, doi:10.1016/S1464-1909(00)00171-4.

Muth, X., M. Schneebeli, and A. Berne, 2012: A sun-tracking method to improve the pointing accuracy of weather radar. *Atmos. Meas. Tech.*, **5**, 547–555, doi:10.5194/amt-5-547-2012.

Pratt, J. F., and D. G. Ferraro, 1989: Automated solar gain calibration. Preprints, *24th Conf. on Radar Meteorology*, Tallahassee, FL, Amer. Meteor. Soc., 619–622.

Puhakka, P., M. Leskinen, and T. Puhakka, 2004: Experiments on using the Sun for radar calibration. *Third European Conference*

on Radar in Meteorology and Hydrology (ERAD) together with the COST 717 Final Seminar, Copernicus, 335–340.

Rico-Ramírez, M. A., E. González-Ramírez, I. Cluckie, and D. Han, 2009: Real-time monitoring of weather radar antenna pointing using digital terrain elevation and a Bayes clutter classifier. *Meteor. Appl.*, **16**, 227–236, doi:10.1002/met.112.

Saltikoff, E., A. Huuskonen, H. Hohti, J. Koistinen, and H. Järvinen, 2010: Quality assurance in the FMI Doppler Weather Radar Network. *Boreal Environ. Res.*, **15**, 579–594.

Sánchez-Diezma Guijarro, R., 2001: Optimización de la medida de lluvia por radar meteorológico para su aplicación hidrológica. Ph.D. thesis, Universitat Politecnica de Catalunya, 330 pp. [Available online at http://www.crahi.upc.edu/en/publications/others/118-tesis.]

——, D. Sempere-Torres, J. Bech, and E. Velasco, 2002: Development of a hydrometeorological flood warning system (EHIMI) based on radar data. *Proceedings of the Second European Conference on Radar Meteorology and Hydrology (ERAD): In Conjunction with COST 717 Mid-Term Seminar*, Copernicus, 619–622.

Tapping, K., 2001: Antenna calibration using the 10.7cm solar flux. *Workshop on Radar Calibration*, Albuquerque, NM, Amer. Meteor. Soc., 32 pp.

Trapero, L., J. Bech, T. Rigo, N. Pineda, and D. Forcadell, 2009: Uncertainty of precipitation estimates in convective events by the Meteorological Service of Catalonia network. *Atmos. Res.*, **93**, 408–418, doi:10.1016/j.atmosres.2009.01.021.

Vaisala, 2014: Utilities manual: IRIS and RDA. Vaisala Oyj M211316EN-D, 320 pp.

Vega, M. A., V. Chandrasekar, C. Nguyen, K. V. Mishra, and J. Carswell, 2012: Calibration of the NASA dual-frequency, dual-polarized, Doppler radar. *IGARSS 2012: IEEE International Geoscience and Remote Sensing Symposium; Remote Sensing for a Dynamic Earth*, IEEE, 4625–4628, doi:10.1109/IGARSS.2012.6350435.

Whiton, R. C., P. L. Smith, and A. C. Harbuck, 1976: Calibration of weather radar systems using the sun as a radio source. Preprints, *17th Conf. on Radar Meteorology*, Seattle, WA, Amer. Meteor. Soc., 60–65.